AGU PUBLICATIONS

JGR

Journal of Geophysical Research: Solid Earth

RESEARCH ARTICLE
10.1002/2016JB012928

Key Points:
- A dipping marine magnetic polarity reversal boundary (C2r.2r/C2An.1n, ~2.581 Ma) is resolved in a fracture zone wall
- The polarity boundary has a west dipping angle of ~45° in the shallow crust and <20° in the deeper crust
- The magnetic polarity boundary represents both a frozen isotherm and an isochron

Correspondence to:
M. Xu,
mxu@scsio.ac.cn

Citation:
Xu, M., and M. A. Tivey (2016), Investigation of a marine magnetic polarity reversal boundary in cross section at the northern boundary of the Kane Megamullion, Mid-Atlantic Ridge, 23°40′N, *J. Geophys. Res. Solid Earth*, *121*, 3161–3176, doi:10.1002/2016JB012928.

Received 16 FEB 2016
Accepted 21 APR 2016
Accepted article online 23 APR 2016
Published online 12 MAY 2016

Investigation of a marine magnetic polarity reversal boundary in cross section at the northern boundary of the Kane Megamullion, Mid-Atlantic Ridge, 23°40′N

Min Xu[1,2] and M. A. Tivey[2]

[1]Key Laboratory of Marginal Sea Geology, South China Sea Institute of Oceanology, Chinese Academy of Sciences, Guangzhou, China, [2]Department of Marine Geology and Geophysics, Woods Hole Oceanographic Institution, Woods Hole, Massachusetts, USA

Abstract Near-bottom magnetic field measurements made by the submersible *Nautile* during the 1992 *Kanaut Expedition* define the cross-sectional geometry of magnetic polarity reversal boundaries and the vertical variation of crustal magnetization in lower oceanic crust exposed along the Kane Transform Fault (TF) at the northern boundary of the Kane Megamullion (KMM). The KMM exposes lower crust and upper mantle rocks on a low-angle normal fault that was active between 3.3 Ma and 2.1 Ma. The geometry of the polarity boundaries is estimated from an inversion of the submarine magnetic data for crustal magnetization. In general, the polarity boundaries dip away from the ridge axis along the Kane TF scarp, with a west dipping angle of ~45° in the shallow (<1 km) crust and <20° in the deeper crust. The existence of the magnetic polarity boundaries (e.g., C2r.2r/C2An.1n, ~2.581 Ma) indicates that the lower crustal gabbros and upper mantle serpentinized peridotites are able to record a coherent magnetic signal. Our results support the conclusion of Williams (2007) that the lower crust cools through the Curie temperature of magnetite to become magnetic, with the polarity boundaries representing both frozen isotherms and isochrons. We also test the effects of the rotation of this isotherm structure and/or footwall rotation and find that the magnetic polarity boundary geometry is not sensitive to these directional changes.

1. Introduction

Oceanic core complexes (OCCs) are sections of oceanic lithosphere exhumed at the seafloor by long-lived normal faults also referred to as "detachment" faults that initiate at mid-ocean ridges (MORs) [*Blackman et al.*, 1998; *Cann et al.*, 1997; *Escartin et al.*, 2008; *MacLeod et al.*, 2002; *Searle et al.*, 2003; *Tucholke et al.*, 1996, 1998]. OCCs provide important "tectonic windows" into sections of oceanic lithosphere that are otherwise confined to the deep subsurface. The Kane Megamullion (KMM) is an OCC located between ~30 and 55 km off axis on the North American Plate, on the western side of the Mid-Atlantic Ridge (MAR) axis, immediately south of the ~150 km long, left stepping Kane transform fault, between ~23°20′N and ~23°40′N (Figure 1). KMM formed between 3.3 Ma and 2.1 Ma based on sea surface magnetic anomaly data, during a period marked by strongly asymmetrical spreading of the MAR spreading center (i.e., 17.9 mm/a on the OCC side on the west and 7.9 mm/a on the conjugate (east) side between chrons C2 and C2A; Figure 2) [*Williams et al.*, 2006]. The seafloor morphology of KMM shows characteristic smooth surfaces and spreading-parallel corrugations typical of megamullions formed by major oceanic detachment faults [*Tucholke et al.*, 1998; *Searle et al.*, 2003].

Long-term movement of the footwall on the detachment fault uplifted and exposed lower crust and upper mantle rocks at the seafloor and can potentially accommodate a significant component of plate motion by extension, even in the absence of magmatism [*Escartín et al.*, 2008; *Tucholke et al.*, 2008]. The abundance of gabbros and altered peridotites exposed along the northern edge of the KMM [*Auzende et al.*, 1994; *Dick et al.*, 2008] is consistent with a positive residual mantle Bouguer gravity anomaly [*Ballu et al.*, 1998; *Maia and Gente*, 1998; *Morris and Detrick*, 1991] and large lateral variations in seismic velocity [*Canales et al.*, 2008; *Xu et al.*, 2009]. These observations indicate that the KMM may be not only an ideal tectonic window where the geological record of mantle flow and melt generation and migration can be studied [*Dick et al.*, 2010] but also an ideal location to define the contribution of gabbro and peridotite to the magnetic anomaly signal [*Williams et al.*, 2006]. A well-defined magnetic anomaly reversal (C2r.2r/C2An.1n, ~2.581 Ma [*Cande and Kent*, 1995]) crosses the KMM from south to north, parallel to the strike of the MAR [*Williams*, 2007], indicating that the lithospheric section

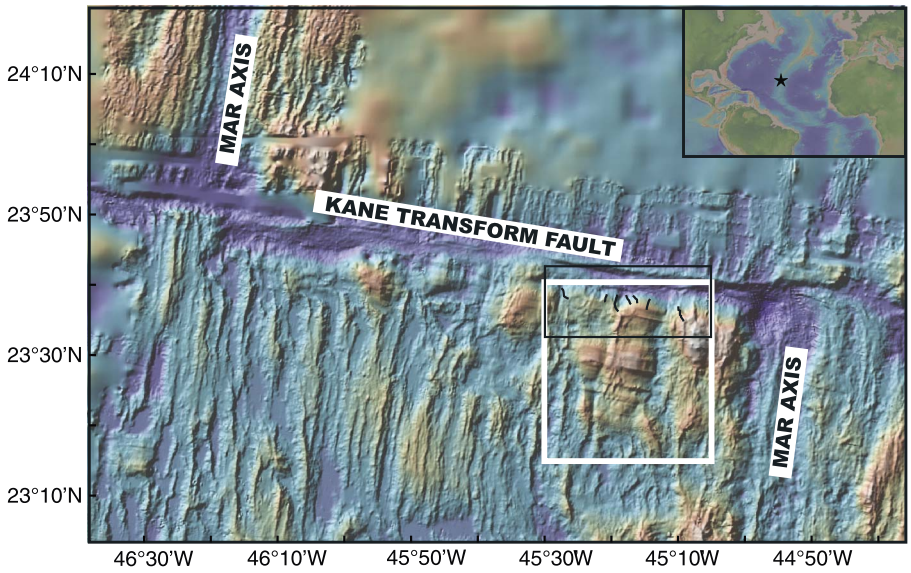

Figure 1. Shaded relief bathymetry of the Mid-Atlantic Ridge (MAR) around the Kane fracture zone from the Marine Geoscience Data System (http://www.geomapapp.org). The star in the inset shows the study location on the MAR. The black box outlines the study area (Figures 2 and 3), the white box outlines the Kane oceanic core complex, and black lines represent the seven magnetic survey profiles that were obtained during the 1992 *Kanaut Expedition* [*Auzende et al*., 1992].

at this location has been able to record and preserve magnetic field polarity signals consistent with a seafloor spreading process [cf. *Morley and Larochelle*, 1964; *Vine and Matthews*, 1963]. The presence of this polarity reversal is remarkable because the underlying lithology has been documented to be dominated by gabbro and peridotite [*Dick et al*., 2008]. The KMM is terminated on its northern boundary by the Kane fracture zone. The relatively steep scarp along the southern wall of the Kane fracture zone provides a good opportunity to measure in situ vertical magnetic structure and to define the nature of the polarity reversal that intersects the Kane

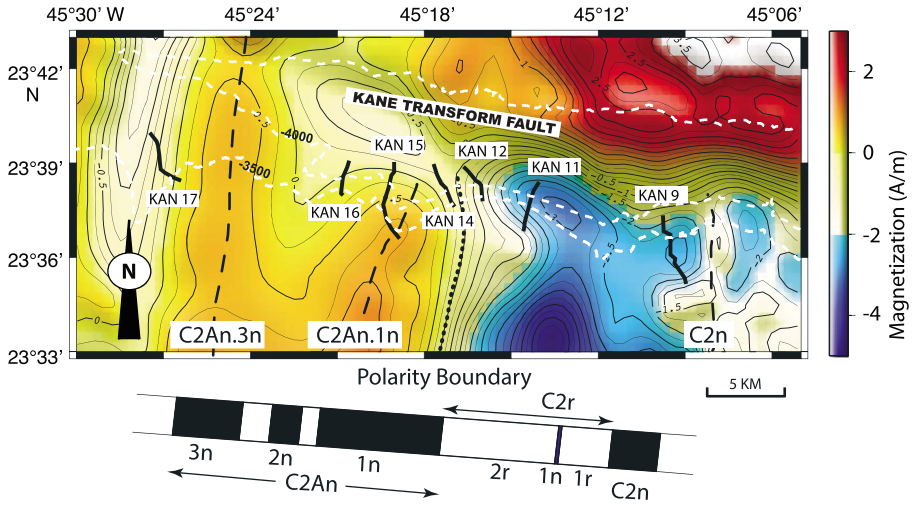

Figure 2. Contoured inversion result of the sea surface magnetic anomaly data around the Kane fracture zone (adapted from *Williams* [2007]) overlain with near-bottom magnetic survey profiles (shown in solid black lines). The contour interval is 0.25 A/m, and every 0.5 A/m is labeled. The Kane transform valley is outlined by two iso-bathymetry contours (shown in white dashed lines), at 3500 m and 4000 m. The geomagnetic polarity timescale (GPTS) of *Ogg* [2012] is projected to the direction perpendicular to the MAR at the bottom of the figure. Chrons C2n and C2An are made up of several subchrons. The black dotted line marks the C2r.2r/C2An.1n polarity boundary, while the black dashed lines locate the possible locations of subchrons C2An.3n, C2An.1n, and Chron C2n. The question mark indicates that the location of Chron C2n is not well resolved by the sea surface magnetic anomaly data.

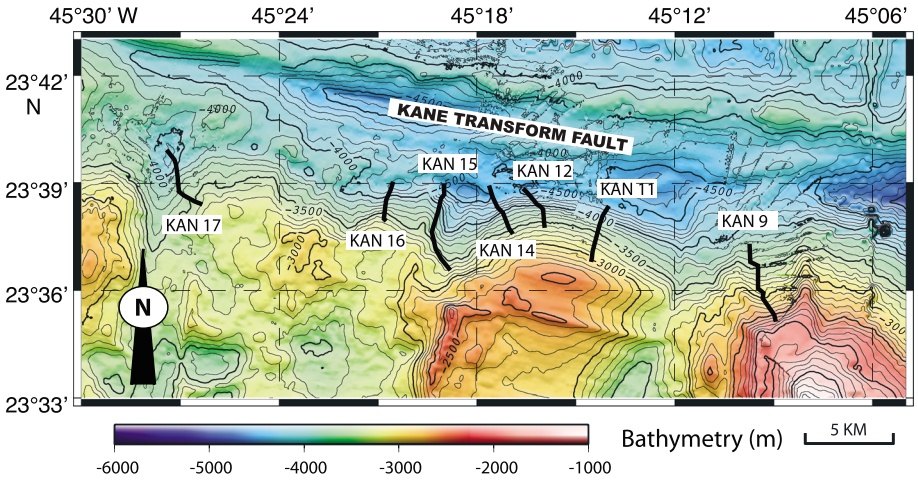

Figure 3. Detailed SeaBeam bathymetry map obtained from R/V *Knorr* Cruise 180-2 (adapted from *Dick et al.* [2008]). The contour interval is 100 m, and every 500 m is labeled. The black lines show the positions of the seven near-bottom magnetic survey lines employed in this study.

transform wall at the KMM. The symmetric distribution of marine magnetic lineations about the axes of MOR provide key evidence for seafloor spreading processes and the theory of plate tectonics [*Morley and Larochelle*, 1964; *Vine and Matthews*, 1963], which states that coherent marine magnetic anomalies are a record of the recurring polarity reversals of the Earth's magnetic field preserved in oceanic crust by seafloor spreading at MORs. However, the geometry and even the existence of polarity boundaries within lower crustal and upper mantle rocks is a subject of debate, speculation, and inference with very little direct information available to test the various models [e.g., *Allerton and Tivey*, 2001; *Blakely*, 1973; *Cande and Kent*, 1976; *Dyment and Arkani-Hamed*, 1995; *Dyment et al.*, 1997; *Kidd*, 1977; *Wilson and Hey*, 1981]. The hypothesis which we consider more reliable suggests that the lower crust (gabbros) cools through its Curie isotherm to become magnetic so that a polarity boundary would represent a frozen isotherm as well as an isochron [e.g., *Williams*, 2007]. A polarity boundary in altered peridotite could be either a result of the progressive migration of upper mantle through an alteration zone as the footwall moves on the detachment fault and thus behaves like an isochron or the upper mantle could become altered at a location and time that has no isochronal relevance. Both the gabbro and peridotite lithologies have the potential to preserve remanent magnetic signals; i.e., they could contribute to the source of the observed magnetic anomaly signal [e.g., *Davis*, 1981; *Gee et al.*, 1997; *Kent et al.*, 1978; *Oufi et al.*, 2002; *Pariso and Johnson*, 1993; *Williams*, 2007]. Thus, the presence and geometry of a polarity boundary at KMM and the Kane transform wall provide an important opportunity to investigate the history and structure of oceanic crust and upper mantle exposed on a detachment fault and to investigate how crustal magnetization may be preserved in these lithospheric sections.

In this paper, we analyze a series of magnetic profiles collected by the submersible *Nautile* vertically up the southern wall of the Kane fracture zone and present the calculated magnetization structure to determine the geometry of a magnetic polarity reversal boundary exposed in cross section on the northern boundary of KMM on the flanks of the MAR near 23°40'N. The final results present obvious magnetization contrasts that vary in position and depth across the scarp face. These magnetization contrasts could arise either from lithological variations (i.e., gabbro versus altered peridotite magnetization intensity) or they could represent true magnetic polarity reversals. We discuss these two possibilities but conclude that the polarity interpretation is the most likely explanation for the observed variation. We correlate these magnetization variations to produce a map of the geometry of the polarity boundary in cross section. Finally, we investigate the impact of footwall rotation on the geometry of polarity boundaries that we obtained from modeling these data.

2. Data Collection

The magnetic data used in this study were acquired during the 1992 *Kanaut Expedition* [*Auzende et al.*, 1993, 1994]. This expedition used the submersible *Nautile* to study the southern wall of the Kane transform zone from its eastern intersection with the MAR to 5 Ma in age [*Auzende et al.*, 1994]. A total of 20 *Nautile* dives were

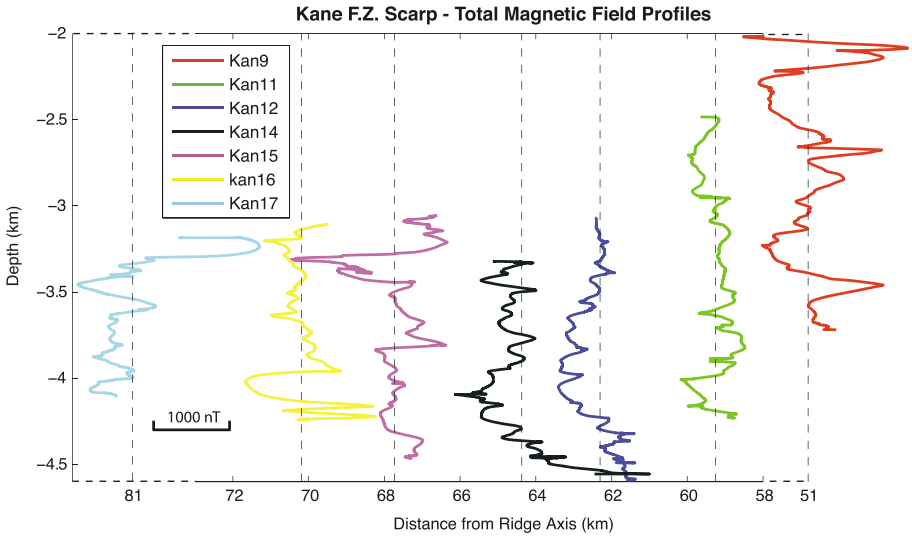

Figure 4. Observed total magnetic field anomaly (nT) profiles plotted versus depth below the sea surface at the approximate lateral distance from the MAR axis. Profiles Kan 9 and Kan 17 are plotted offset from their true location as shown by dashed lines to better compare all the profiles.

conducted, including 10 at the eastern ridge-transform intersection and the inside corner massif and 10 along the southern wall of the Kane transform zone between 45°08′W and 45°28′W. Here we present results from seven *Nautile* dives (KAN 9, 11, 12, 14, 15, 16, and 17) conducted where the transform wall forms the northern boundary of the KMM [*Auzende et al.*, 1993, 1994; *Ghose et al.*, 1996] (Figures 1 and 3). Magnetic field data were collected using a three-axis fluxgate magnetometer (Alvin magnetometer manufactured by IFG) mounted to the front sample basket of *Nautile*. Data were recorded inside the submersible on a laptop computer and later combined with depth, heading, and altitude, which were simultaneously recorded by the *Nautile* data system. Depth and altitude were measured to an accuracy of ±0.1 m. Submersible navigation used a ship-based acoustic transponder net with an estimated *X-Y* relative accuracy of ±10 m. The measured three-axis magnetic field components were vector summed for total field, because no independent orientation data were available for vector analysis. The near-bottom measurements along the relatively steep Kane transform scarp allow us to record vertical magnetic profiles (Figure 4) that were used in magnetic inverse modeling. Magnetic field data were corrected for the permanent and induced magnetic fields of the submersible by using a Nelder-Mead algorithm [*Press et al.*, 1986] to minimize the total magnetic field variations measured during spins of the submersible on the descent and ascent of each dive. In order to estimate a correct heading function, a heading correction technique was used to correct for the submersible contribution because digital submersible pitch and roll data were not available. The residual noise levels were generally below 200 nT in amplitude and insignificant compared to the geophysical signals of several thousands of nanoteslas. Finally, the 12th Generation International Geomagnetic Reference Field [*Thébault et al.*, 2015] for year 1992 was removed from the magnetic data. Magnetic field measurements, obtained at a 1 Hz sampling rate and with a relative accuracy of ±0.1 nT, were typically obtained at a variable altitude from a few meters to a few hundred meters above the Kane scarp because of the local scarp topography and the overall convex-shaped scarp face. Short-wavelength magnetic anomaly spikes arise during the rock sampling process. The sample basket at the submersible swings out to allow samples to be stored, and the manipulators come close to the magnetic sensor during these operations, which imparts magnetic field distortions. To eliminate these short-wavelength anomalies, we deleted these sampling periods from the magnetic record (Figure 4).

3. Methods

3.1. Vertical Magnetic Profile Analysis

The vertical magnetic profiling (VMP) approach [*Tivey*, 1996; *Tivey et al.*, 1998] is used to analyze the magnetic field data collected along transections up the Kane transform scarp where exposures of oceanic upper lithosphere are found. This approach assumes that remanent magnetization dominates over induced magnetization, i.e., that the crustal rocks have a relatively high Koenigsberger ratio as we document later. The relatively

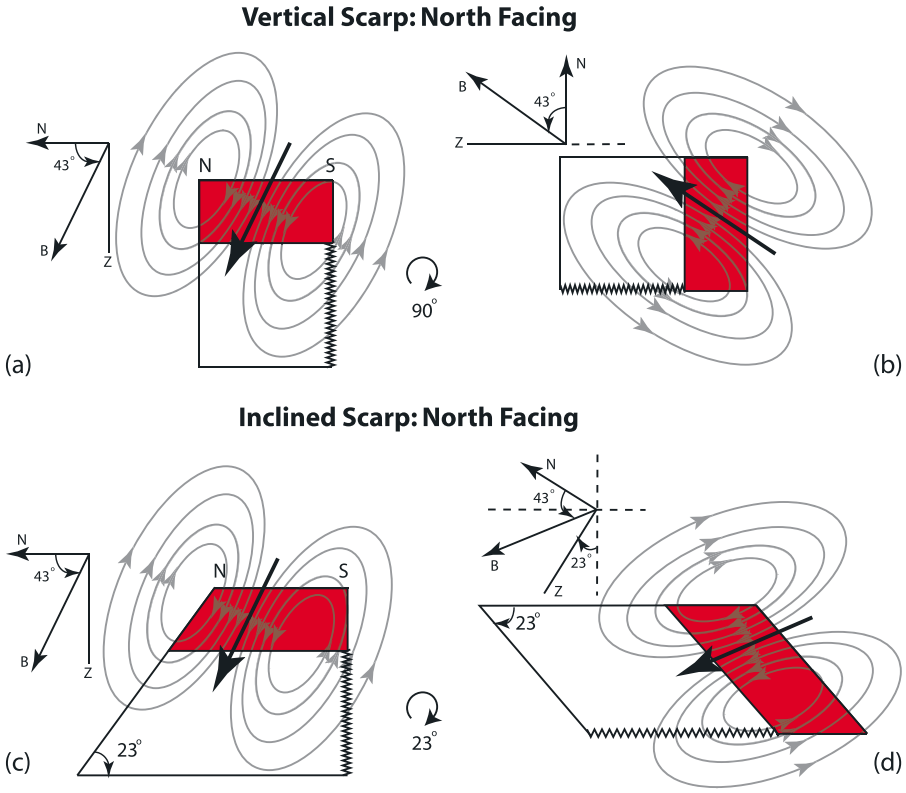

Figure 5. A cartoon showing the rotation of the coordinate systems used in the analysis of the vertically oriented magnetic data (modified from *Tivey* [1996]). (a) The conventional coordinate orientation showing a north facing vertical scarp face oriented east-west with a magnetized layer (shaded in red color) extending to the south. (b) The vertical scarp face shown in Figure 5a has been rotated into the horizontal so that the magnetization layer now extends to infinite depth. In this orientation vertical boundaries indicate that the phase shift is due to field and magnetization inclinations. (c) A scarp face with a 23° slope and a magnetized layer (shaded in red color) in the conventional orientation. (d) The sloping scarp face shown in Figure 5c has been rotated into the horizontal with an angle equal to the slope angle. Note the magnetized layer now dips with an angle equal to the slope angle, which adds to the phase shift due to the field and magnetization inclinations.

steep geometry of these escarpments provides an excellent tectonic window to map the vertical magnetic structure and stratigraphy of oceanic lithosphere [e.g., *Karson et al*., 1992; *Tivey*, 1996; *Tivey et al*., 1998]. To demonstrate the vertical magnetic profile analysis approach, we assume the simplest geometry of a single fault with a monotonic slope and calculate the predicted anomaly that would arise for the north facing Kane transform wall measurements.

Conventional analysis of marine magnetic field data collected over the seafloor assumes that the magnetic source region is composed of crustal prisms of finite thickness and of infinite length perpendicular to the profile [e.g., *Parker*, 1973; *Schouten and McCamy*, 1972; *Vacquier*, 1962]. This layered model is a good approximation of normal oceanic crustal structure, but the nonuniqueness of the magnetic inversion method means that either the source layer thickness or magnetization can be determined, but not both. Typically, a constant thickness source layer is assumed to obtain a vertically averaged crustal magnetization for the layer [*Parker and Huestis*, 1974]. This approach has worked well within the overall framework of oceanic crustal structure that has been derived from ophiolite, crustal drilling, and seismic studies [e.g., *Granot et al*., 2006; *Henstock et al*., 1995; *Schouten and Denham*, 1979]. In the vertical magnetic profile case, the geometry of layered oceanic crust can be used to advantage in order to calculate the magnetic response of the source layer. Magnetic measurements adjacent to a vertical scarp face (Figure 5a) can be viewed in a new, rotated reference frame, where the scarp face is rotated into the horizontal (Figure 5b). The original geomagnetic field and magnetization vectors are also rotated within this new reference frame. In this rotated coordinate system, a reasonable and realistic approximation can be made that the oceanic crust is composed of a series of thin tabular bodies, perpendicular to the profile and extending to infinite depth. If we assume that the magnetic anomalies are two dimensional and strike

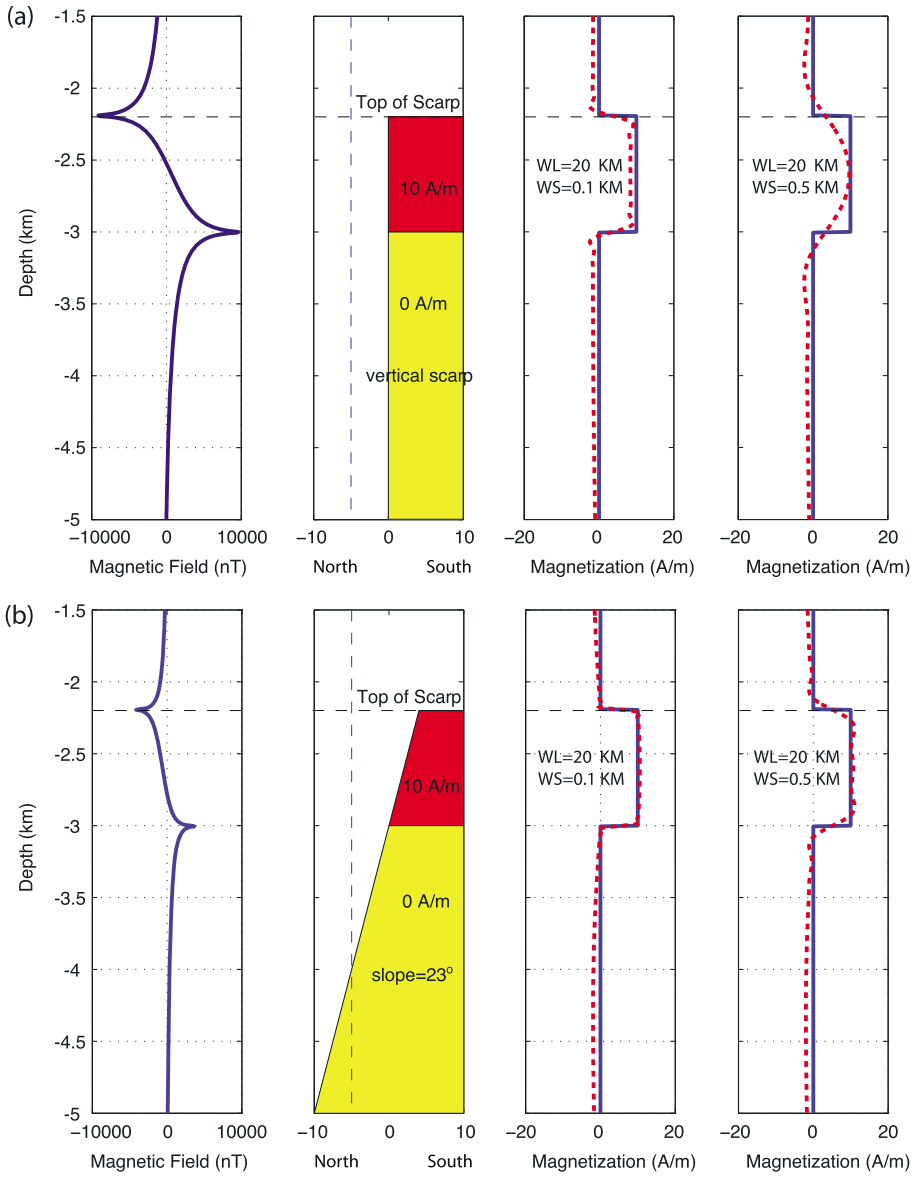

Figure 6. Forward and inverse magnetic modeling obtained from the vertical magnetic profile analysis of (a) vertical scarp face and (b) sloping scarp face with an angle of 23°. The rotated magnetic field and magnetization inclinations are 47°, and declinations are −17° and 0°, respectively. The survey height is assumed to be 5 m over the scarp, and the magnetization of the crust is assumed to be 10 A/m for the upper 800 m and nonmagnetic for the lower crustal section. In each case, (left) computed magnetic field, the resultant asymmetric magnetic field has a magnetic low at the top, indicating reversed polarity and a magnetic high at the transition from the magnetic layer to the nonmagnetic layer. (middle left) Scarp face model and magnetized layer (shaded in red color). (middle right) The blue line shows the input magnetization, and the red dashed line shows the inverted magnetization using a band-pass filter for wavelengths from 0.1 km to 20 km. (right) The same as middle right, showing the comparison of input and inverted magnetization using a band-pass filter for wavelengths from 0.5 km to 20 km.

along the scarp perpendicular to profile (Figure 5b), we can use analytical and Fourier transform solutions [*Gay*, 1963; *Pedersen*, 1978; *Tivey*, 1996] to calculate the resultant magnetic field. We can also carry out an inversion of the magnetic field for crustal magnetization using the same reference frame. In general, the zero level of the magnetization contrast can be fixed by using the contrast of nonmagnetic seawater with the top of the scarp. The direction of magnetization remains unknown so that a geocentric dipole direction must be assumed, as in conventional analysis. As with other nonlinear inversion techniques, however, solutions are nonunique so that an infinite number of magnetization solutions may exist.

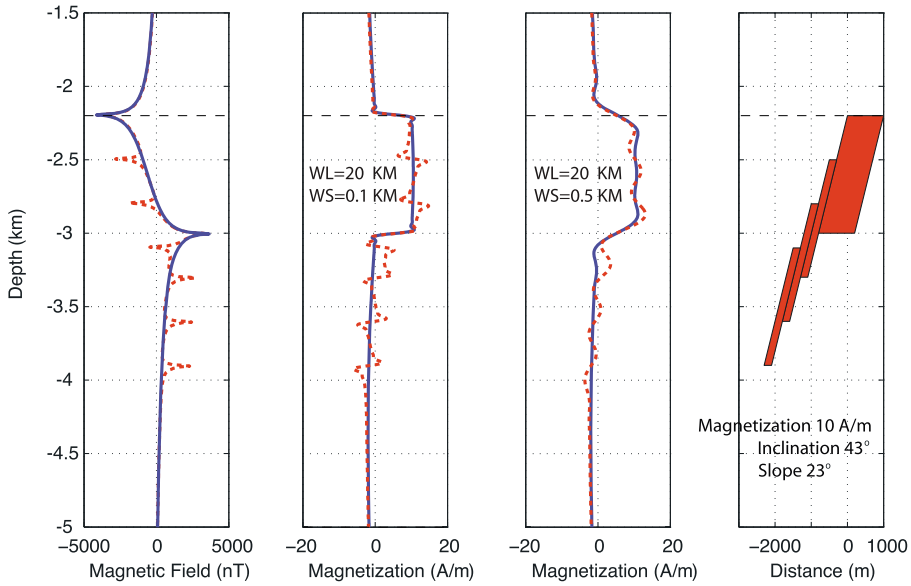

Figure 7. Forward magnetic model showing the effect of faulted blocks upon the magnetic signal. (right) A model with an upper intact block and three slipped blocks, all with a 10 A/m normal polarity magnetization and a slope angle of 23°. (left) Calculated magnetic field: solid line represents the field due to a single intact block without the slipped blocks, and the red dashed line represents the field due to the integrated effect of all blocks. Note that magnetic lows align with the top of blocks and magnetic highs with the toe of blocks. (middle left) Inversion of the calculated magnetic field for crustal magnetization using a band-pass filter of wavelength range from 0.1 km to 20 km: solid line is the inversion for the single intact block, while the red dashed line is for the integrated inversion of all the blocks. (middle right) The same as middle left but using a different band-pass filter of wavelength range from 0.5 km to 20 km for inversion. Note that there is a complex relationship between magnetization and the blocks. Magnetization highs correlated to where the fault blocks overlap, reacting to the effective thickness of the magnetized layer.

For the more realistic case of a nonvertical scarp face, e.g., with a slope of 23° (the same value as the averaged slope of all seven dive profiles used in this study; Figure 5c), the scarp face is rotated into the horizontal by an amount equal to the slope angle (Figure 5d). In this case, instead of vertically oriented tabular bodies, source bodies are dipping with an angle equivalent to the slope in the new coordinate system (Figure 5d), which introduces an additional phase shift into the anomaly. This rotation is merely to facilitate the mathematical analysis and has no physical meaning for crustal rotation.

3.2. A Test Case Example of Forward and Inverse Modeling

To demonstrate the feasibility of magnetic measurements along a scarp we construct two forward models in which we make no inferences about crustal structure but merely show what we expect from a single horizontally layered magnetized body (Figure 6). The survey height is assumed to be 5 m over the scarp and the magnetization of the crust is assumed to be 10 A/m for the upper 800 m and nonmagnetic for the lower crustal section. For the vertical scarp (Figure 6a), the combination of scarp slope angle (90°) and geomagnetic field inclination +43° means that the effective magnetic field has a new inclination direction of −47° (i.e., equivalent to being in the southern hemisphere), and it provides a sufficiently large contrast to generate anomalies on the order of 10,000 nT at 5 m distance from the scarp for a 10 A/m magnetization contrast (Figure 6a). For the nonvertical scarp face (Figure 6b), the combination of scarp slope angle (23°) and geomagnetic field inclination +43° indicates that the effective magnetic field has a shallow inclination of +20°, which is enough to generate somewhat weaker anomalies on the order of 4000 nT at 5 m distance from the scarp for a 10 A/m magnetization contrast (Figure 6b). Remember also that in this case the source body dips at an angle of 23° rather than being vertically oriented, thus imparting an additional phase shift.

Inversion for crustal magnetization can be obtained from the synthetic magnetic field data assuming that the dipping bodies extend to effectively infinite "depth." Note that both the forward and inverse models assume a level topography and observation plane. The inversion assumes that all the layers' dip with the same angle

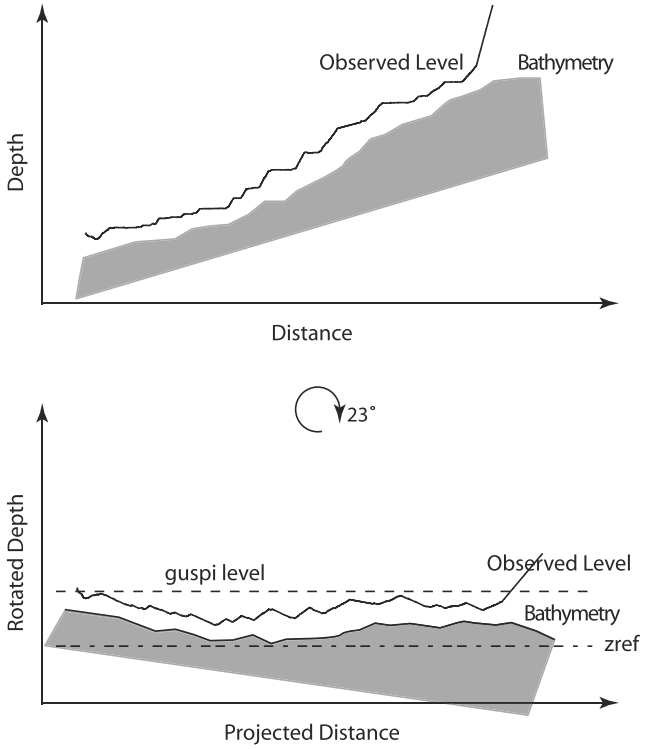

Figure 8. A cartoon shows the Guspi upward continuation procedure to reduce magnetic measurements made on an uneven surface to a level plane [*Guspi*, 1987]. First of all, the observed level is rotated clockwise to a horizontal plane, i.e., with an average scarp angle 23° in this paper. The resultant magnetic field data are then downward continued to a constant water-depth plane (zref), i.e., an equivalent plane, to remove the effects of variations in vehicle altitude. Finally, the magnetic field data are upward continued to a water depth (guspi level), such that all of the bathymetry in the survey lies below this depth.

and that the layers extend to infinity with constant magnetization within the layers [*Tivey*, 1996]. The inverted magnetization profiles can be compared with the input models (Figure 6). As with any potential field measurement, the depth that the VMP technique effectively "samples into the wall" is wavelength dependent, with longer wavelengths representing greater penetration of the wall and shorter-wavelength features representing surficial and topographic signals [*Tivey*, 1996]. Figure 6 shows two inversions with different wavelength band-pass filters: 0.1–20 km and 0.5–20 km. The 0.5 km cutoff results in a smoother inversion than predicted so that it cannot fully resolve the sharp change between the two different magnetic layers. We also note that for inversions with the same filter (0.1–20 km or 0.5–20 km), the nonvertical scarp case (with a slope angle of 23°) appear to fit the input magnetization much better than the vertical scarp case. This is caused by the different geometry of the two model scarps. For the sloping scarp model, rotation results in an effectively wider source body that separates the two edge effects of the magnetized body, and this reduces their interference. As in all near-bottom survey techniques, the short averaged length of the profile of ~3.5 km in this study limits the longest wavelengths that can be reliably sampled.

The magnetic effect of a single magnetized block while useful is perhaps too simple. Thus, we constructed a more complicated model attempting to model a series of slipped fault blocks akin to a "slipped deck of cards" [*Francheteau et al.*, 1979]. This may be particularly important for scarps that are composed of repeated crustal sections (Figure 7). We compute the magnetic field for a conceptual model, where an upper, highly magnetized crustal section is faulted 3 times, producing three slipped blocks. The resultant magnetic field is shown for the upper magnetized unit alone and then for all the units (Figure 7). As can be seen from the forward model, each slipped block produces a short-wavelength magnetic anomaly with anomaly highs at the toe of each block and anomaly lows at the top of each block. The intact block at the top gives an overall longer-wavelength signature. The forward modeled magnetic field was inverted for crustal magnetization to simulate our data analysis steps using two different wavelength band-pass filters, 0.1–20 km and 0.5–20 km (Figure 7). Both inversions show that the overall positive magnetization of the upper block is recognizable as a long-wavelength positive zone, while the slipped blocks give a less intuitive result. The short-wavelength magnetization highs reflect the variable thickness of the source layers due to the overlapping of the blocks, rather than any amplitude difference in magnetization. Note also that the profile shows zones of reversely magnetized crust where there are normal polarity blocks (e.g., ~4 km deep in Figure 7) for both filters. These models (Figures 6 and 7) are meant to serve as a guide to interpreting our observed magnetic profiles rather than to explicitly fit them. The direct submersible observations on the southern Kane transform wall find, however, that the wall has an overall convex morphology with no evidence of any repeated lithologic sections [*Auzende et al.*, 1992, 1994; *Dick et al.*, 2008].

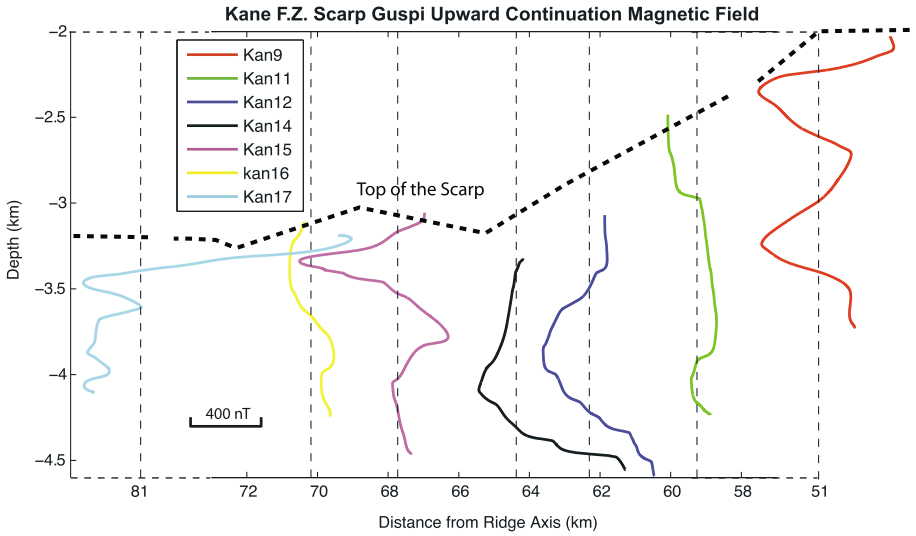

Figure 9. The computed Guspi upward continuation magnetic profiles plotted versus depth at the approximate lateral distance from the MAR axis. The magnetic profiles are calculated using an iterative fast Fourier transform based on the method of *Guspi* [1987]. The required upward continuation levels are set to four data points spacing above the minimum depth of each profile.

4. Data Processing and Results

We applied the VMP approach described above to the magnetic profiles measured on the Kane transform wall in the KMM area. For the seven *Nautile* magnetic lines used in this paper, we first edited out bad data points at rock sampling stations (as described in section 2) and then smoothed the data using a 100-point moving average window (~100 m) after equal-spaced interpolation. The magnetic profiles were then projected into the direction parallel to the strike of the MAR axis, perpendicular to the general strike of the scarp. An average slope of 23° was used to represent the slope angle of the Kane scarp. Because the magnetic data were obtained along an uneven surface just above the convex-shaped scarp, we must upward continue the observed magnetic field data to a level plane above the seafloor topography. We use an iterative fast Fourier transform approach to obtain this upward continued field [*Guspi*, 1987; *Pilkington and Urquhart*, 1990]. Figure 8 shows the geometry necessary to reduce the magnetic measurements made on an uneven surface to a level plane. First of all, the observed level (i.e., dive track) is rotated clockwise to a horizontal plane with an angle of 23° that is equivalent to the average scarp slope. The resultant magnetic field data were then upward continued to a constant water-depth plane above the topography to remove the effects of variations in submersible altitude [*Guspi*, 1987]. The resultant upward continued magnetic profiles are shown in Figure 9, and all the profiles, in general, exhibit clear variations up the scarp. The profiles were then inverted for magnetization using a modified Fourier transform approach for the analysis of dipping tabular bodies, assuming the semiinfinite source [*Tivey*, 1996; *Tivey et al.*, 1998]. A band-pass wavelength filter from 0.5 km to 20 km was used to filter out short-wavelength anomalies that presumably arise from local bathymetric sources and submersible motion and which do not affect the main magnetic signal that we seek. The filtering also helps in the convergence of the inversion solution [*Tivey*, 1994]. The root-mean-square (RMS) errors were used to measure the differences between observed magnetic field and synthetic field predicted by the inverted crustal magnetization; e.g., the RMS value was reduced to 173.34, 84.00, 206.13, 45.28, 175.37, 179.52, and 110.55 nT for profiles Kan 9, 11, 12, 14, 15, 16, and 17, respectively, during the inversion process, indicating that the observed magnetic field was properly modeled.

A summary of the inverted crustal magnetization profiles for the Kane scarp study area is shown in Figure 10. The nonuniqueness of the inversion solution is represented by the annihilator function, which is a magnetization that produces no external field. An infinite amount of annihilator may be added to the solution without affecting the resultant magnetic field. In our result, unfortunately, we cannot locate the accurate positions of the magnetization contrast between the top of the scarp and the overlying nonmagnetic seawater; thus, we only adjusted the solution profiles so that the maximum and minimum magnetization values of each profile

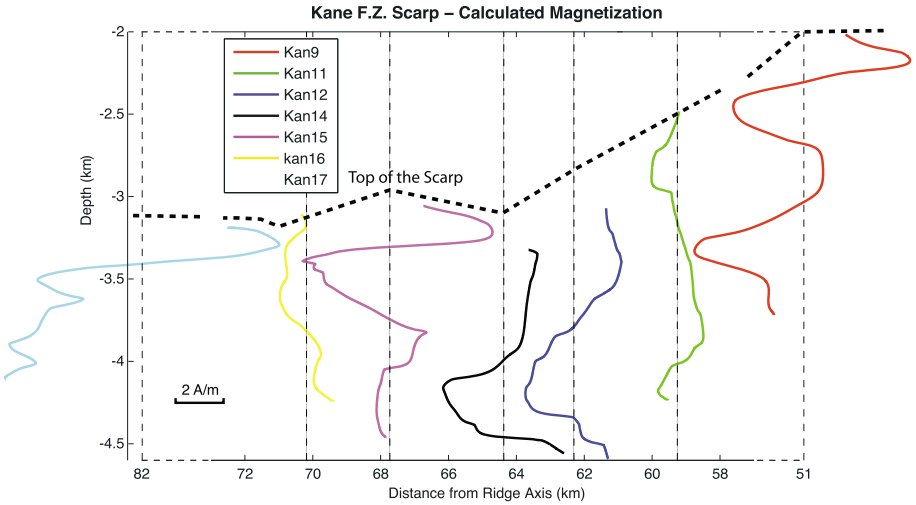

Figure 10. Inverted magnetization profiles plotted versus depth at the approximate lateral distance from the MAR axis. Note that the strong vertical variations in magnetization are required to fit the observed magnetic data (Figure 4) and are not just simply consistent with the observed data.

were balanced. These magnetization inversions show alternating zones of magnetization intensity that appear to correlate laterally between profiles (Figure 10). The magnetization of all the profiles ranges from approximately −4 A/m to 4 A/m, which is roughly consistent with the magnetization values obtained from sea surface data (Figure 2) and paleomagnetic analysis of representative rock samples [*Williams*, 2007; *Williams et al*., 2006].

5. Discussion

The computed magnetization profiles from the northern scarp of the KMM (Figure 10) show variations that appear to correlate laterally among the profiles. However, because there is an ambiguity in the actual magnitude of the magnetization (i.e., the zero magnetization level), we must address two potential end-member explanations for the source of these observed variations. The first explanation is that these magnetization variations simply represent lithological variations, specifically that we are documenting weakly magnetized formations in contrast to more strongly magnetized formations; i.e., there is no polarity information contained in these profiles. If on the other hand the observed magnetization variations represent true polarity differences, then the lateral correlation of these units have some isochronal significance. Below we discuss the relative merits of these two cases.

5.1. The Case for a Lithological Source

Here we discuss the possibility that the magnetization variations we find are the result of lithological variations. We concentrate our correlation analysis on four dives (Kan 11, 12, 14, and 15) that form relatively complete transections up the south wall of the Kane transform located on the northern part of KMM (Figure 3). The four dives together provide a relatively continuous transect over the interpreted magnetic polarity boundary C2r.2r/C2An.1n (Figure 2). In situ submersible observations and rock samples suggest that the Kane scarp is composed primarily of gabbros and serpentinized peridotites (Figure 11) [*Auzende et al*., 1994; *Dick et al*., 2008].

We create a magnetization-lithology correlation by mapping the magnetization solution profiles and the interpreted lithological distributions [*Dick et al*., 2008] along the dive tracks (Figure 11). However, because we cannot unambiguously define the magnetization polarity (zero magnetization level), we may only discuss the correlation with relatively weak and strong magnetization instead of positive and negative magnetizations. If we take −4 to +4 A/m as the range in inverted magnetization, then this translates to 0 to +8 A/m, with 0 A/m indicating the weakest magnetization and +8 A/m indicating the strongest magnetization. The magnetization profiles are projected on the top of the scarp face to compare with the lithological distributions in Figure 11. At the bottom of profile Kan 11, serpentinized peridotites correlate with weak magnetization.

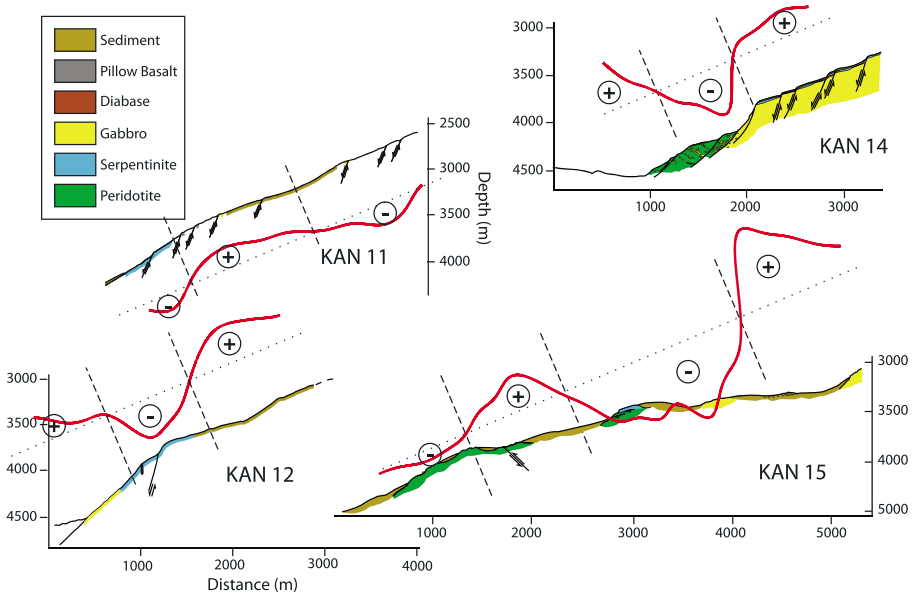

Figure 11. Comparison of projected inverted magnetization structures and lithologies of four dive profiles, Kan 11, 12 14, and 15. The lithological distribution map is adopted from *Dick et al.* [2008]. The dotted lines mark the 0 A/m in inverted magnetization or translated magnitude 4 A/m. The dashed lines represent the interpreted strongly (labeled as circled "+") and weakly (labeled as circled "−") magnetized boundaries.

Along profile Kan 12, the serpentinized peridotite section correlates with weak magnetization, while the gabbro section at the bottom of the profile shows somewhat stronger magnetization. Gabbros along the upper section of profile Kan 14 correlate with strong magnetization, while a peridotite section at the bottom of the profile shows magnetization increasing downward. Profile Kan 15 shows a more complicated lithological distribution and magnetization structure, and our data resolution does not allow us to infer a clear correlation. Peridotite sections correlate mostly with weak magnetization; however, a small gabbro section at the top of the profile shows strong magnetization, while a gabbro section near the middle of the profile shows weak magnetization. A clear correlation cannot be deduced between the magnetization and lithology and/or between strongly and weakly magnetized boundaries and the positions that show lithological transitions (Figure 11). However, it is still interesting to notice that most gabbro sections are showing stronger magnetizations (e.g., on the top of profile Kan 14 and bottom of profile Kan 12), except the middle gabbro section of profile Kan 15, while most (serpentinized) peridotites are showing weaker magnetizations (e.g., on the bottom of profiles Kan 11 and 15 and in the middle section of profiles Kan 12 and Kan 14).

The range in translated magnetization from 0 to +8 A/m is greater than the paleomagnetic results of *Williams*' [2007] work and other measurements of gabbro and serpentinized peridotite rocks [*Gee et al.*, 1997; *Kent et al.*, 1978; *Oufi et al.*, 2002; *Pariso and Johnson*, 1993]. Also, the relatively weak and strong magnetization of gabbro and peridotite shown in Figure 11 is not consistent with previous rock magnetic and paleomagnetic results from the KMM, which indicate that serpentinized peridotites have higher mean natural remanent magnetizations (4.7 ± 5.8 A/m) compared to the gabbros (1.5 ± 2.5 A/m), although both are capable of carrying a remanent magnetization of geomagnetic origin and the gabbros are more stable and have a higher Koenigsberger ratio than the peridotites [*Williams*, 2007].

The magnetization-lithology correlation investigated here is strongly based on the seafloor surficial geological interpretation [*Auzende et al.*, 1994; *Dick et al.*, 2008]. Thus, it is not necessarily indicative of deeper phases of more major lithology variations. We should also note that we used a short-wavelength cutoff (0.5 km) during the magnetization inversion, which means that the high-frequency magnetic signal resulting from shallower lithologic units is filtered out and that only broad-scale changes are effectively imaged. If the lithological distribution does influence the observed magnetization, it is most likely that the latter primarily reflects the magnetic polarity structure as described below.

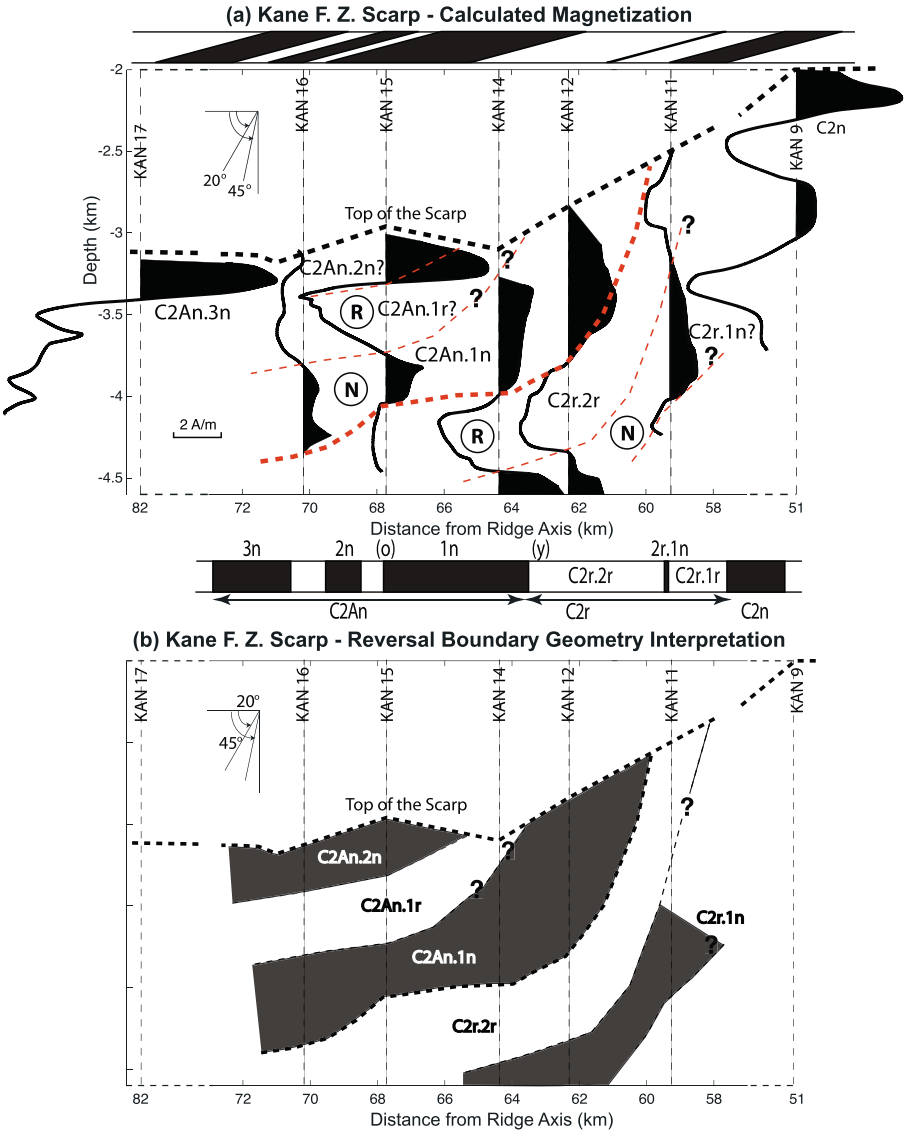

Figure 12. (a) Summary diagram of the inverted magnetization profiles plotted versus depth for the Kane scarp study area at approximately the horizontal distance from the MAR axis. Kan 9 and Kan 17 are plotted offset from their true location as shown by dashed lines to better compare all the profiles. Dive numbers are labeled on the top of each profile. Positive magnetized sections are filled in black. A conceptual dipping GPTS of *Ogg* [2012] is projected on the top of the figure, and another normal GPTS is projected at the bottom of the figure. Label *o* on bottom GPTS represents old side, while *y* represents young side. The black dashed line roughly outlines the top of the scarp. The thick red dashed line outlines the main polarity boundary of subchrons C2r.2r/C2An.1n, while the thin red lines represent other subchron boundaries. All of the possible corresponding subchrons are labeled along each magnetization profile. Question marks indicate that the local interpretation was made without full confidence. (b) Simplified reversal boundary geometry interpretation along the Kane scarp on the basis of Figure 12a. Other features are as described in Figure 12a. The interpreted polarity boundary dips away from the ridge axis, with a west dipping angle ~45° in the shallow crust and <20° in the deeper crust.

5.2. The Case for a Polarity Source

We now describe the calculated magnetization variations in terms of polarity variation and discuss the arguments that support and perhaps refute this interpretation. If we assume that the magnetization variations are representative of polarity variations, then the first observation we can make is that all the magnetization profiles show alternatively positive and negative magnetizations that are consistent with the geomagnetic polarity timescale (GPTS) subchrons [*Ogg*, 2012] projected from the sea surface magnetic interpretation

framework (Figure 12a). The magnetization structures of the middle five profiles were used to simulate the polarity boundary geometry according to the sequence of the GPTS subchrons [*Ogg*, 2012]. The boundary of chrons C2An and C2r (~2.581 Ma) appears to be well defined underneath the fault scarp with a shallow west dipping angle, roughly estimated to be ~45° in the shallow crust and <20° in the deeper crust (Figure 12). Question marks in Figure 12 indicate the location where we are not fully confident, interpreting the geometry because of the broad spacing of the profiles and the corresponding potential subchron interpretations. Another two magnetic profiles were obtained a little further from the northern margin of KMM. The eastern profile Kan 9 was obtained near the normal Chron C2n, and the western profile Kan 17 was measured near the normal subchron C2An.3n, determined on the basis of the GPTS of *Ogg* [2012].

The sea surface inversion results over the KMM [*Williams*, 2007] clearly show the lineated anomalies formed at the MAR (Figure 2). Based on the regional magnetic lineations, the interpreted magnetic reversal boundaries in Figure 12b represent the period between subchrons C2r.2r (2.148–2.581 Ma) and C2An.2n (3.116–3.207 Ma). Chron C2An is composed of three normal subchrons, C2An.1n, C2An.2n, and C2An.3n, but the sea surface inversion results indicate that only two subchrons, possibly the two longer ones, C2An.1n (2.581–3.032 Ma) and C2An.3n (3.33–3.596 Ma), are clearly resolved by the sea surface data. From sea surface data, the C2An.1n (young) boundary (Figure 12a) is linear in appearance at the southern wall of the Kane transform fault, but it is not well defined north of 23°40′N (Figure 2), indicating that the lineated anomalies are truncated by the Kane fracture zone. Chron C2n (1.778–1.945 Ma) is resolved by the sea surface data (Figure 2), but the shorter subchron C2r.1n (2.128–2.148 Ma) is not resolved by the sea surface data. In general, our vertical magnetization models resolve all of the subchrons within and between the chrons C2An and C2n (Figure 12a), including those represented by subchron C2An.3n shown in profile Kan 17; subchron C2An.1n shown in profiles Kan 12, 14, 15, and 16; the relative short subchron C2An.2n shown along the top of profile Kan 15 with some uncertainty; subchron C2r.1n in profiles Kan 11 and Kan 12 with some uncertainty; and Chron C2n at the top of profile Kan 9.

The crustal magnetization inversion solution across the magnetic reversal boundary calculated from the sea surface data varies from about −3 to 1 A/m in the direction of increasing age, assuming a nominal 1 km thick source layer and geocentric axial dipole direction (inclination is 40° and declination is 0°; Figure 2) [*Williams*, 2007]. However, because our magnetization solution along each profile was obtained only by balancing the maximum and minimum magnetization amplitudes, our results cannot resolve the absolute magnetization values across the polarity boundary without an accurate zero magnetization level. Note that the magnetization profile of dive Kan 12, showing positive magnetization on the top of the scarp, is shifted some distance from the subchron C2An.1n. This discrepancy can be caused by the dipping geometry of the polarity boundary underneath the scarp [*Tivey et al*., 1998]. Furthermore, the sea surface data inversion solution (Figure 2) and GPTS subchrons (Figure 12a) only represent the average magnetization structure beneath the scarp, although a nominal 1 km thick source layer was assumed for inversion. Thus, we would also not expect a good comparison between the shallow magnetization amplitudes and the surface data inversion solution and GPTS.

5.3. Magnetic Polarity Reversal Boundary

The interpreted geometry of the polarity reversal boundary of chrons C2An/C2r (Figure 12b) shows that both the normal section of subchron C2An.1n and the reversal section of subchron C2r.2r are recorded along the middle five profiles. The polarity boundary dips west away from the ridge axis with an angle of ~45° in the shallow (<1 km) crust and <20° in the deeper crust. The interpretation of how the reversal boundary formed is important for understanding the history and structure of oceanic crust and upper mantle.

There is not a solid correlation between the magnetization structure and the lithology (see section 5.1), so we can rule out the possibility that the geomagnetic reversal boundary was exclusively formed by the lithological changes even though gabbros and serpentinized peridotites show different magnetic characteristics. If we consider an isotherm model that is consistent with the frozen cooling isotherm hypothesis for the source of polarity boundaries in gabbro, then the isotherm should dip away from the spreading center. The analysis of *Williams* [2007] resolves the dip angle of the boundary using an analytic signal technique applied to near-bottom autonomous vehicle Autonomous Benthic Explorer profiles and suggests a dip of 46°W ± 14° for the northern region of KMM. This is roughly consistent with our shallow interpretation (~45°) along the Kane scarp.

The frozen cooling isotherm is formed as the gabbroic crustal section cools through the magnetite Curie temperature of 580°C. The footwall rotates when exposed by the detachment faulting, and the rotation results

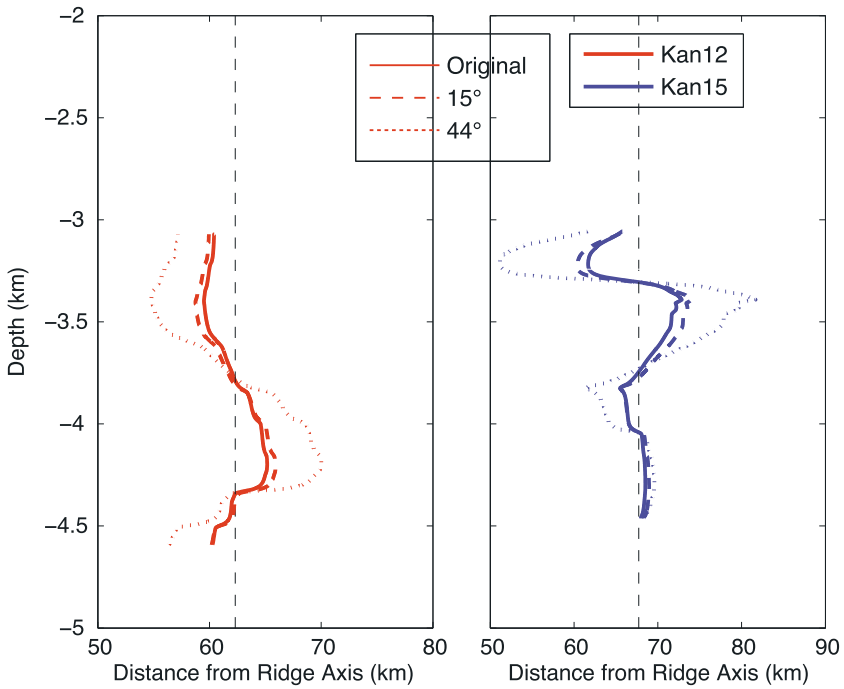

Figure 13. Comparison of inverted magnetization profiles after 15° and 44° rotations with the original inverted magnetization for two dive profiles, Kan 12 and Kan 15. All of the calculations assumed that the samples acquired their magnetization prior to the footwall rotation and with the initial inclination of 43° and declination of 0°.

in a more steepened magnetization vector and frozen polarity boundary. According to the temperature structure calculation of *Williams* [2007], the isotherm of 580°C has an initial dip angle of 13°, but after footwall rotation, the dip angle becomes 57°, indicating a 44° of rotation. Rotation angles have also been estimated in other OCCs using paleomagnetic vectors from drill cores. *Garcés and Gee* [2007] used the remanence vector in core complex gabbros from the 15°20′N region as a measure of the rotation, assuming that the samples acquired their magnetization prior to deformation and their vectors remained as passive markers during subsequent rotation of the footwall. Their results suggest rotations of 50°–80° in 1 Ma old crust. A similar study conducted by *Carlut et al.* [2006] from footwall samples at 15°45′N shows rotations of ~40°. Similarly, *Morris et al.* [2009] used reoriented core and formation microscanner well logs to show a 46° outward rotation of the gabbroic section drilled at Atlantis Massif. Conversely, *Szitkar and Dyment* [2015] suggest a 53° rotation in the hanging wall from magnetic anomalies at TAG. Estimates from the limited paleomagnetic data suggest that the KMM has only experienced approximately 15° of counterclockwise rotation [*Williams*, 2007].

For our analysis we assumed a geocentric axial dipole (GAD) direction for magnetization in the absence of any other information. We can, however, calculate the effect of such footwall rotations of a GAD direction. The initial recorded magnetization was assumed to have a GAD inclination of 43° and declination of 0°. The rotated inclination and declination can be calculated following the method of *Verosub and Moores* [1981] for footwall rotation about an axis parallel to the strike of the MAR. Inverted magnetization profiles of dives Kan 12 and Kan 15 using the new parameters after a 15° rotation (calculated from the paleomagnetic data [*Williams*, 2007]) and a 44° rotation (calculated from the temperature structure) are compared with the original inverted profiles in Figure 13. The three sets of magnetization profiles share the same shape although with some amplitude variations. After footwall rotation of 44°, the inverted magnetizations are exaggerated more than twice of their original value (Figure 13). Thus, the 44° footwall rotation produces an unrealistic magnetization amplitude which is also not compatible with the observation data. However, while the amplitude changes, the depth position of the magnetization contrasts does not change. Therefore, our polarity reversal interpretation is not sensitive to these directional changes. Nevertheless, the magnetic vector direction is an important aspect of this work; in order to achieve the accurate inclination and declination required to resolve the footwall rotation angles oriented drill hole samples would be necessary.

6. Conclusions

We present an analysis of legacy submersible magnetic data collected in 1992 using the deep submersible *Nautile* on the fracture zone scarp of the Kane Megamullion in the Atlantic. These data were collected during a time when such measurements were in an experimental stage, and so the data set has limited short-wavelength ability to resolve outcrop-scale magnetization that might resolve unambiguous magnetic polarity of outcrops [e.g., *Honsho et al.*, 2009; *Szitkar et al.*, 2015]. Nevertheless, our detailed study of these submersible magnetic profiles from the exposed crustal section of the Kane scarp shows that the longer-wavelength components of the lateral variation in crustal magnetization as a function of depth can be mapped and directly related to the overlying lineated anomaly signal measured at the sea surface. This variation suggests that the contributions of gabbros and (serpentinized) peridotites to the magnetic source layer are significant, but our data cannot resolve the relative contributions. A dipping magnetic polarity boundary can be interpreted from the magnetization variations within the crustal sequence, and it is compatible with the location of boundary of subchrons C2An.1n and C2r.2r (~2.581 Ma). The interpreted polarity boundary has an ~45° dipping angle in the shallow crust which is consistent with estimates from rock magnetic and paleomagnetic solutions, while there is a relatively shallow dipping angle (<20°) in the deeper crustal section. Our result is consistent with the prevailing hypothesis that lower crust (gabbros) cool through magnetite Curie isotherm to become magnetic so that a magnetic polarity boundary would represent both a frozen isotherm and an isochron. Our polarity reversal boundary interpretation does not depend on the rotation angle of the KMM footwall.

Acknowledgments

We thank the captain, crew, and scientific party of R/V *Kanaut Expedition* Cruise for their efforts in making the *Nautile* magnetic surveys a success. We thank L. Cocchi and J. Dyment for their thoughtful and insightful comments and suggestions. We also thank H. Dick and B. Tucholke for generously sharing the geologic sample data on KMM with us. M. Tivey participated in the *Kanaut Expedition*, and particularly, thanks to Chief Scientist J. M. Auzende who invited M. Tivey to participate in the cruise. Finally, we thank the *Kanaut* scientific party for a well-documented cruise report. The inversion results and original magnetic field data are available upon request via e-mail to the corresponding author.

References

Allerton, S., and M. A. Tivey (2001), Magnetic polarity structure of the lower oceanic crust, *Geophys. Res. Lett.*, *28*, 423–426.

Auzende, J.-M., M. Cannat, P. Gent, J.-P. Henriet, T. Juteau, J. Karson, Y. Lagabrielle, and M. A. Tivey (1992), Rapport de la Campagne Kanaut du Nautille sur le N/O Nadir, *Sci. Rep.*, 426.

Auzende, J.-M., M. Cannat, P. Gente, J.-P. Henriet, T. Juteau, J. A. Karson, Y. Lagabrielle, C. Mével, and M. A. Tivey (1993), Affleurements des roches profondes de la croûte océanique et du manteau sur le mur sud de la fracture Kane (Atlantique central): Observations par submersible, *C. R. Acad. Sci. Paris*, *317*, 1641–1648.

Auzende, J.-M., M. Cannat, P. Gente, J.-P. Henriet, T. Juteau, J. A. Karson, Y. Lagabrielle, C. Mével, and M. A. Tivey (1994), Observation of sections of oceanic crust and mantle cropping out on the southern wall of Kane FZ (N. Atlantic), *Terra Nova*, *6*, 143–148, doi:10.1111/j.1365-3121.1994.tb00647.x.

Ballu, V., J. Dubois, C. Deplus, M. Diament, and S. Bonvalot (1998), Crustal structure of the Mid-Atlantic Ridge south of the Kane fracture zone from seafloor and sea surface gravity data, *J. Geophys. Res.*, *103*, 2615–2631, doi:10.1029/97JB02542.

Blackman, D. K., J. R. Cann, B. Janssen, and D. K. Smith (1998), Origin of extensional core complexes: evidence from the Mid-Atlantic Ridge at Atlantis Fracture Zone, *J. Geophys. Res.*, *103*, 21,315–21,333.

Blakely, R. J. (1973), An age-dependent, two-layer model for marine magnetic anomalies, in *The Geophysics of the Pacific Ocean Basin and Its Margin, Geophys. Monogr. Set*, vol. 19, pp. 227–234, AGU, Washington, D. C.

Canales, J. P., B. E. Tucholke, M. Xu, J. A. Collins, and D. L. Dubois (2008), Seismic evidence for large-scale compositional heterogeneity of oceanic core complexes, *Geochem. Geophys. Geosyst.*, *9*, Q08002, doi:10.1029/2008GC002009.

Cande, S. C., and D. V. Kent (1976), Constraints imposed by the shape of marine magnetic anomalies on the magnetic source, *J. Geophys. Res.*, *81*, 4157–4162.

Cande, S. C., and D. V. Kent (1995), Revised calibration of the geomagnetic timescale for the Late Cretaceous and Cenozoic, *J. Geophys. Res.*, *100*, 6093–6095.

Cann, J. R., D. K. Blackman, D. K. Smith, E. McAllister, B. Janssen, S. Mello, E. Avgerinos, A. R. Pascoe, and J. Escartín (1997), Corrugated slip surfaces formed at ridge-transform intersections on the Mid-Atlantic Ridge, *Nature*, *385*, 329–332, doi:10.1038/385329a0.

Carlut, J., C. J. MacLeod, H. Horen, and J. Escartin (2006), *Paleomagnetic Results from a Mid-Ocean Ridge Detachment at the Mid-Atlantic Ridge, 15°45'N*, *EGU Meeting*, Vienna.

Davis, K. E. (1981), Magnetite rods in plagioclase as the primary carrier of stable NRM in ocean floor gabbros, *Earth Planet. Sci. Lett.*, *55*, 190–198.

Dick, H. J. B., M. A. Tivey, and B. E. Tucholke (2008), Plutonic foundation of a slow-spread ridge segment: The oceanic core complex at Kane Megamullion, 23°30'N, 45°20'W, *Geochem. Geophys. Geosyst.*, *9*, Q05014, doi:10.1029/2007GC001645.

Dick, H. J. B., C. J. Lissenberg, and J. M. Warren (2010), Mantle melting, melt transport, and delivery beneath a slow-spreading ridge: The paleo-MAR from 23°15'N to 23°45'N, *J. Petrol.*, *51*(1-2), 425–467, doi:10.1093/petrology/egp088.

Dyment, J., and J. Arkani-Hamed (1995), Spreading-rate-dependent magnetization of the oceanic lithosphere inferred from the anomalous skewness of marine magnetic anomalies, *Geophys. J. Int.*, *121*(3), 789–804.

Dyment, J., J. Arkani-Hamed, and A. Ghods (1997), Contribution of serpentinized ultramafics to marine magnetic anomalies at slow and intermediate spreading centres: Insights from the shape of the anomalies, *Geophys. J. Int.*, *129*, 691–701.

Escartín, J., D. K. Smith, J. Cann, H. Schouten, C. H. Langmuir, and S. Escrig (2008), Central role of detachment faults in accretion of slow-spreading oceanic lithosphere, *Nature*, *455*, 790–794, doi:10.1038/nature07333.

Francheteau, J., P. Choukroune, R. Hekinina, X. Le Pichon, and H. D. Needham (1979), Oceanic fracture zones do not provide deep sections in the crust, *Canadian J. Earth Sci.*, *13*(9), 1223–1235.

Garcés, M., and J. Gee (2007), Paleomagnetic evidence of large footwall rotations associated with low-angle faults at the Mid-Atlantic Ridge, *Geology*, *35*(3), 279–282.

Gay, S. P. J. (1963), Standard curves for interpretation of magnetic anomalies over long tabular bodies, *Geophysics*, *28*, 161–200.

Gee, J. S., R. M. Lawrence, and S. D. Hurst (1997), Remanence characteristics of gabbros from the MARK area: Implications for crustal magnetization, *Proc. Ocean Drill. Program Sci. Results*, *153*, 429–436.

Ghose, I., M. Cannat, and M. Seyler (1996), Transform fault effect on mantle melting in the MARK area (Mid-Atlantic Ridge south of the Kane Transform), *Geology*, *24*, 1139–1142.
Granot, R., M. Abelson, H. Ron, and A. Agnon (2006), The oceanic crust in 3D: Paleomagnetic reconstruction in the Troodos ophiolite gabbro, *Earth and Planet. Sci. Lett.*, *251*, 280–292.
Guspi, F. (1987), Frequency-domain reduction of potential field measurements to a horizontal plane, *Geologija*, *24*, 87–98.
Henstock, T. J., R. S. White, and J. H. McBride (1995), The OCEAN study area: Tectonic history from magnetic anomaly data and seismic reflectivity, *J. Geophys. Res.*, *100*(B10), 20,059–20,078.
Honsho, C., J. Dyment, K. Tamaki, M. Ravilly, H. Horen, and P. Gente (2009), Magnetic structure of a slow spreading ridge segment: Insights from near-bottom magnetic measurements on board a submersible, *J. Geophys. Res.*, *114*, B05101, doi:10.1029/2008JB005915.
Karson, J. A., J. R. Delaney, F. N. Spiess, S. D. Hurst, B. Lawhead, S. Bigger, D. D. Naidoo, and P. Gente (1992), Deep-tow operations at the eastern intersection of the Mid-Atlantic Ridge and the Kane fracture zone paper presented at 1992 Fall Meeting, AGU, Washington, D. C., 27 October.
Kent, D. V., et al. (1978), Magnetic properties of dredged oceanic gabbros and source of marine magnetic anomalies, *Geophys. J. R. Astron. Soc.*, *55*, 513–537.
Kidd, R. G. W. (1977), The nature and shape of the sources of marine magnetic anomalies, *Earth Planet. Sci. Lett.*, *33*, 310–320.
MacLeod, C. J., et al. (2002), Direct geological evidence for oceanic detachment faulting: The Mid-Atlantic Ridge, 15°45′N, *Geology*, *30*(10), 879–882.
Maia, M., and P. Gente (1998), Three-dimensional gravity and bathymetry analysis of the Mid-Atlantic Ridge between 20°N and 24°N: Flow geometry and temporal evolution of the segmentation, *J. Geophys. Res.*, *103*, 951–974, doi:10.1029/97JB01635.
Morley, L. W., and A. Larochelle (1964), Paleomagnetism as a means of dating geological events, in *Roy. Soc. Can. Spec. Publ*, vol. 8, pp. 39–50.
Morris, A., J. S. Gee, N. Pressling, B. E. John, C. J. MacLeod, C. B. Grimes, and R. C. Searle (2009), Footwall rotation in an oceanic core complex quantified using reoriented Ocean Drilling Program core samples, *Earth Planet. Sci. Lett.*, *287*, 217–228.
Morris, E., and R. S. Detrick (1991), Three-dimensional analysis of gravity anomalies in the MARK area, Mid-Atlantic Ridge 23°N, *J. Geophys. Res.*, *96*, 4355–4366, doi:10.1029/90JB02173.
Ogg, J.G. (2012), Geomagnetic polarity time scale, in *The Geologic Time Scale 2012*. edited by F. M. Gradstein et al., pp. 85–113, Elsevier, Netherlands, doi:10.1016/B978-0-444-59425-9.00005-6.
Oufi, O., M. Cannat, and H. Horen (2002), Magnetic properties of variably serpentinized abyssal peridotites, *J. Geophys. Res.*, *107*(3-1), 2095, doi:10.1029/2001JB000549.
Pariso, J. E., and H. P. Johnson (1993), Do lower crustal rocks record reversals of the Earth's magnetic field? Magnetic petrology of oceanic gabbros from Ocean Drilling Program Hole 735B, *J. Geophys. Res.*, *98*(981), 16,013–16,032.
Parker, R. L. (1973), The rapid calculation of potential anomalies, *Geophys. J. R. Astron. Soc.*, *31*, 447–455.
Parker, R. L., and S. P. Huestis (1974), The inversion of magnetic anomalies in the presence of topography, *J. Geophys. Res.*, *79*, 1587–1593.
Pedersen, L. B. (1978), A statistical analysis of potential fields using a vertical cylinder and a dike, *Geophysics*, *43*, 943–953.
Pilkington, M., and W. E. S. Urquhart (1990), Reduction of potential field data to a horizontal plane, *Geophysics*, *55*(5), 549–555.
Press, W. H., B. P. Flannery, S. A. Teukolsky, and W. T. Vetterling (1986), *Numerical Recipes: The Art of Scientific Computing*, vol. 818, Cambridge Univ. Press, Cambridge, U. K.
Schouten, H., and C. Denham (1979), Modeling the oceanic magnetic source layer paper presented at Deep drilling results in the Atlantic Ocean: Ocean crust: Maurice Ewing Series.
Schouten, H., and K. McCamy (1972), Filtering marine magnetic anomalies, *J. Geophys. Res.*, *77*, 7089–7099.
Searle, R. C., M. Cannat, K. Fujioka, C. Mevel, H. Fujimoto, A. Bralee, and L. M. Parsons (2003), FUJI Dome: A large detachment fault near 64°E on the very-slow spreading Southwest Indian Ridge, *Geochem. Geophys. Geosyst.*, *4*(25), doi:10.1029/2009GC002497.
Szitkar, F., and J. Dyment (2015), Near-seafloor magnetics reveal tectonic rotation and deep structure at the TAG (trans-Atlantic geotraverse) hydrothermal site (Mid-Atlantic Ridge, 26°N), *Geology*, *43*(1), 87–90.
Szitkar, F., J. Dyment, Y. Fouquet, Y. Choi, and C. Honsho (2015), Absolute magnetization of the seafloor at a basalt-hosted hydrothermal site: Insights from a deep-sea submersible survey, *Geophys. Res. Lett.*, *42*, doi:10.1002/2014GL062791.
Thébault, E., et al. (2015), International Geomagnetic Reference Field: The 12th generation, *Earth, Planets Space*, *67*(79), doi:10.1186/s40623-015-0228-9.
Tivey, M. A. (1994), Fine-scale magnetic anomaly field over the southern Juan de Fuca Ridge: Axial magnetization low and implications for crustal structure, *J. Geophys. Res.*, *99*(B3), 4833–4855.
Tivey, M. A. (1996), Vertical magnetic structure of ocean crust determined from near-bottom magnetic field measurements, *J. Geophys. Res.*, *101*, 20,275–20,296.
Tivey, M. A., H. P. Johnson, C. Fleutelot, S. Hussenoeder, R. Lawrence, C. Waters, and B. Wooding (1998), Direct measurement of magnetic reversal polarity boundaries in a cross-section of oceanic crust, *Geophys. Res. Lett.*, *25*(19), 3631–3634.
Tucholke, B. E., J. Lin, and M. C. Kleinrock (1996), Mullions, megamullions, and metamorphic core complexes on the Mid-Atlantic Ridge *Eos Trans. AGU*, *77*, *Fall Meet. Suppl.*, F724.
Tucholke, B. E., J. Lin, and M. C. Kleinrock (1998), Megamullions and mullion structure defining oceanic metamorphic core complexes on the Mid-Atlantic Ridge, *J. Geophys. Res.*, *103*, 9857–9866, doi:10.1029/98JB00167.
Tucholke, B. E., M. D. Behn, R. Buck, and J. Lin (2008), The role of melt supply in detachment faulting and the formation of oceanic core complexes, *Geology*, *36*(6), 455–458, doi:10.1130/G24639A.
Vacquier, V. (1962), A machine method for computing the magnetization of a uniformly magnetized body from its shape and a magnetic survey, in *Benedum Earth Magnetism Symposium*, pp. 123–127, Univ. of Pittsburgh Press, Pittsburgh.
Verosub, K. L., and E. M. Moores (1981), Tectonic rotations in extensional regimes and their paleomagnetic consequences for oceanic basalts, *J. Geophys. Res.*, *86*, 6335–6349.
Vine, F. J., and D. H. Matthews (1963), Magnetic anomalies over oceanic ridges, *Nature*, *199*, 947–949.
Williams, C. M. (2007), Oceanic lithosphere magnetization: Marine magnetic investigations of crustal accretion and tectonic processes in mid-ocean ridge environments, PhD thesis, 254 pp., Woods Hole Oceanogr. Inst., Woods Hole.
Williams, C. M., M. A. Tivey, and M. D. Behn (2006), The magnetic structure of Kane megamullion: Results from marine magnetic anomalies, paleomagnetic data and thermal modeling *Eos Trans. AGU*, *87*(*52*), Fall Meet. Suppl., Abstract T42A-03.
Wilson, D. S., and R. N. Hey (1981), The Galapagos axial magnetic anomaly: Evidence for the Emperor Event within the Brunhes and for a two-layer magnetic source, *Geophys. Res. Lett.*, *8*(10), 1051–1054.
Xu, M., J. P. Canales, B. E. Tucholke, and D. L. DuBois (2009), Heterogeneous seismic velocity structure of the upper lithosphere at Kane oceanic core complex, Mid-Atlantic Ridge, *Geochem. Geophys. Geosyst.*, *10* Q10001, doi:10.1029/2009GC002586.